Coalescence of Membrane Tethers: Experiments, Theory, and Applications

Damien Cuvelier,* Imre Derényi,† Patricia Bassereau,* and Pierre Nassoy*
*Laboratoire de Physico-Chimie Curie, Institut Curie, F-75005 Paris, France; and †Department of Biological Physics, Eötvös University, H-1117 Budapest, Hungary

ABSTRACT Tethers are nanocylinders of lipid bilayer membrane, arising in situations ranging from micromanipulation experiments on synthetic vesicles to the formation of dynamic tubular networks in the Golgi apparatus. Relying on the extensive theoretical and experimental works aimed to understand the physics of individual tethers formation, we addressed the problem of the interaction between two nanotubes. By using a combination of micropipette manipulation and optical tweezers, we quantitatively studied the process of coalescence that occurred when the separation distance between both vesicle-tether junctions became smaller than a threshold length. Our experiments, which were supported by an original theoretical analysis, demonstrated that the measurements of the tether force and angle between tethers at coalescence directly yield the bending rigidity, κ, and the membrane tension, σ, of the vesicles. Contrary to other methods used to probe the bending rigidity of vesicles, the proposed approach permits a direct measurement of κ without requiring any control of the membrane tension. Finally, after validation of the method and proposal of possible applications, we experimentally investigated the dynamics of the coalescence process.

INTRODUCTION

Giant unilamellar vesicles, which are readily observed and manipulated under a microscope, are conventionally accepted to be the simplest model that approximates some properties of cellular membranes. In particular, because a number of biological processes involve membrane deformation, fusion, or remodeling (e.g., exocytosis, endocytosis, cell division), it has become apparent that studies of the mechanical properties of artificial lipid vesicles are invaluable for understanding such cellular processes. A general theoretical framework for describing the elastic properties of vesicles has been developed for the last three decades (Evans and Skalak, 1980; Döbereiner et al., 1997). Among other material features, a fundamental macroscopic property of lipid bilayers is the surface bending elasticity, which is closely related to the overall vesicle shape, the molecular chemistry of phospholipids, the temperature, the nature of structural phases (from fluid to gel-like), etc. (Evans and Needham, 1987; Needham and Zhelev, 1996). Furthermore, because lipid bilayers are molecularly thin, their curvature modulus or bending rigidity, κ, is generally extremely small (typically between 10 and 100 times the thermal energy k_BT) and difficult to measure experimentally. There are two well-established methods to determine κ. The first one is flicker spectroscopy where moduli are extracted from the observation of thermally induced shape undulations by light microscopy (Brochard and Lennon, 1975; Faucon et al., 1989). The second one is based on the micropipette technique and relies on the analysis of the relative change in area under aspiration pressure (Evans and Rawicz, 1990; Rawicz et al., 2000).

More recently, Heinrich and Waugh (1996) proposed an innovative micropipette-based approach that exploits the spectacular deformation of vesicles into thin (~10–100 nm) tubes, known as tethers, when a highly localized load is applied. These tethers were first observed to be formed from red blood cells attached to glass surfaces and subjected to hydrodynamic flows (Hochmuth et al., 1973). Later, tubulovesicular networks were reported to be formed both in vivo and in vitro by membrane-associated motors moving along microtubules (Terasaki et al., 1986; Vale and Hotani, 1988; Dabora and Sheetz, 1988; Roux et al., 2002; Koster et al., 2003). Recently, it has been shown that cells can use membrane tethers for intercellular communication (Rustom et al., 2004). Sheetz and co-workers have also shown that tethers can be extracted from neuronal growth cones and other cells with optical tweezers and were able to measure the extrusion force as a function of length (Dai and Sheetz, 1995, 1999; Hochmuth et al.,1996). In all cases, tethers were shown to be mainly membraneous, i.e., devoid of cytoskeleton (Waugh and Bauserman, 1995; Sheetz, 2001). Considerable theoretical and experimental efforts were thus pursued to gain insight into the mechanics of tube formation (Evans and Yeung, 1994; Svetina et al., 1998; Heinrich et al., 1999; Powers et al., 2002; Derényi et al., 2002). From this point of view, the abovementioned method developed by Heinrich and Waugh (1996) was especially instructive. By varying the membrane tension of a vesicle with a micropipette and pulling a tether from this vesicle with a micron-size bead manipulated with a magnetic tweezer, the authors clearly demonstrated that the equilibrium tether force

Submitted November 18, 2004, and accepted for publication January 27, 2005.

Address reprint requests to Dr. Pierre Nassoy, E-mail: pierre.nassoy@curie.fr.

© 2005 by the Biophysical Society

0006-3495/05/04/2714/13 $2.00

doi: 10.1529/biophysj.104.056473

increases with the square root of the tension and that the slope yields the bending rigidity, as expected from theoretical calculations (Waugh and Hochmuth, 1987; Evans and Yeung, 1994).

However, the latter mechanical approach of single tether extraction also opens two important questions. First, like the other two techniques used to determine bending rigidities, this method is especially well adapted to fluid membranes characterized by κ-values of the order of 10–20 k_BT, for which the aspirated tongue in the low tension regime is long enough to relate precisely the aspiration pressure to the membrane tension (i.e., for high membrane area/volume ratio). When vesicles are in a liquid-ordered or gel-like state, for which κ may exceed 100 k_BT (Dimova et al., 2000; Lee et al., 2001), these methods usually fail in determining reliably the bending rigidity. An obvious problem to be addressed then consists in developing a novel method to measure the bending stiffness of any type of phospholipid membranes in the absence of any membrane tension measurement. Second, most of the quantitative studies on tethers were performed on individual tubes. However, on the one hand, tethers are rarely isolated in biological conditions (Terasaki et al., 1986; Upadhyaya and Sheetz, 2004), and on the other hand, networks of membrane tubes have already been built for biotechnological applications (Evans et al., 1996; Karlsson et al., 2002, 2003a,b; Davidson et al. 2003). A second obvious question to be asked is, then, how do these tubes interact with each other? Coalescence of tethers has already been observed by two groups (Evans et al., 1996; Lobovkina et al., 2004). To our knowledge, the mechanism of tube merging has never been experimentally studied and quantitatively described.

At first sight, these two problems, which respectively aim to understand the physics of tether coalescence and to provide a new method to measure the bending rigidities of bilayers, may seem to be independent. Yet, this twofold goal is precisely the main objective of this work. In this article, we present an in-depth analysis of tube merging experiments and demonstrate how controlled coalescence of tethers can be used to measure the bending rigidity of phospholipid vesicles. More concretely, we have implemented an experimental setup based on a dual micropipette manipulation and an optical tweezer, which allows us: 1), to pull two tethers from a giant vesicle, 2), to vary the mutual distance between both vesicle-tube junctions, and 3), to measure the force applied by one tether during extraction. We will show that both the bending rigidity and the surface tension of the vesicle can be directly obtained from the measurement of the angle between the two tubes and the trapping force when coalescence occurs. The feasibility of this approach will be demonstrated on well-characterized fluid vesicles. The method will be critically compared with other well-established techniques and extended to: i), the measure of bending moduli of vesicles in a liquid-ordered phase, and ii), the measure of the surface tension of adhering vesicles. All these experimental results will be analyzed in the framework of new predictions presented in the Theory section. Finally, we will present some preliminary results about the dynamics of coalescence.

MATERIALS AND METHODS

Chemicals and materials

Lipids (egg phosphatidylcholine (EPC), brain sphingomyelin (BSM), 1,2-dioleyl-*sn*-glycero-3-phosphoethanolamine-*N*-[methoxy(polyethyleneglycol)-2000] (mPEG-DOPE), cholesterol, 1,2-distearoyl-*sn*-glycero-3-phosphoethanolamine-*N*-[biotinyl(polyethylene glycol) 2000] (DSPE-PEG-biotin)) were purchased from Avanti Polar Lipids (Alabaster, AL). All other chemicals were purchased from Sigma Aldrich (St. Louis, MO). Streptavidin-coated polystyrene beads (radius $R = 1.76$ μm), which served as handles to pull tethers from vesicles, were purchased from Bangs Laboratories (Carmel, IN).

Vesicle preparation

Giant vesicles were grown using the electroformation technique (Angelova and Dimitrov, 1988). Electroswelling was carried out in a solution of sucrose (170 mOsm) to enhance optical contrast in microscopy observations. Two kinds of vesicles were prepared. Mixtures of EPC/mPEG-DOPE/DSPE-PEG-biotin (95:4.995:0.005) were used to produce vesicles in a liquid-disordered (L_d) phase. The mechanical properties of EPC-based vesicles are well known and their bending rigidity can be easily measured by both prevalent methods (i.e., micropipette aspiration or single tether pulling). This kind of vesicle will then serve to validate our approach. However, because the measurement of the bending modulus of more rigid vesicles is more challenging (as shown below), we have also prepared vesicles in a liquid-ordered (L_O) phase from mixtures of BSM/cholesterol/mPEG-DOPE/DSPE-PEG-biotin (47.5:47.5:4.995:0.005). Electroformation was performed at 50°C (i.e., above the melting temperature of sphingomyelins) to ensure good mixing of lipids during the growth process. As shown by Roux et al. (2005) and by Almeida et al. (2003) for a similar lipid composition, this composition of lipids yields vesicles that do not exhibit phase separation. In both cases, the biotinylated lipid served to make vesicles sticky for streptavidin-coated beads, and the PEG-lipid was used to prevent nonspecific adhesion between bead and vesicle and to get a better control of the contact area. The vesicles obtained in this way were usually large, with diameters from 10 to 100 μm, and the majority of them appeared to be unilamellar. At the beginning of all micromanipulation experiments, the vesicles were resuspended in a PBS + 0.5% β-casein solution. Osmolarity was set at 180 mOsm so that vesicles were flaccid before micropipette aspiration. Addition of casein was aimed to inhibit strong adhesion of vesicles to the bottom glass slide of the observation chamber.

Observation chamber and microscopy

Sample chambers were made of two cleaned glass coverslips glued with vacuum grease and sealed with nail polish to an aluminum support (1-mm thick). The chamber was first filled with the vesicle suspension. Then, streptavidin beads were injected and dispersed in the chamber. Finally, the chamber was placed on the stage of an inverted microscope (Axiovert 200, Zeiss, Jena, Germany). The microscope was equipped with a 100× immersion oil objective (1.3 N.A.), and a 0.8 air numerical aperture condenser. Transmission bright-field images were collected by a charge-coupled device (CCD) camera (XC-ST70CE, Sony, Japan) and recorded at 25 frames per second with a video cassette recorder (SVO-95000MDP, Sony, Japan) after contrast enhancement (Argus image processor, Hamamatsu, Japan).

Micropipette manipulation

The micropipette aspiration technique used to hold vesicles was described elsewhere (Needham and Zhelev, 1996). Briefly, borosilicate capillaries (0.7/1.0 mm inner/outer diameter; Kimble, Vineland, NJ) were first pulled into needles with a horizontal laser puller (P-2000, Sutter Instrument, Novato, CA), then cut open and microforged (DMF1000, World Precision Instruments, Aston, UK) at desired inside diameters (4–4.5 μm). The micropipette was filled with PBS 180 mOsm + casein 0.5% w/w and attached to the chucks on a manipulator, which was mounted on the side of the microscope stage. The micromanipulator was composed of a mechanical three-axis translator (M-105, Physik Instrumente, Karlsruhe, Germany) and a piezoelectric translator (P-783.ZL, 300 μm scanning range, Physik Instrumente), which was placed in series with the coarse x axis, for fine displacement. Control of the piezo was performed through an arbitrary waveform generator (TGA1241, Thurlby Thandar Instruments, UK).

The suction pressure in the vesicle-holding pipette was controlled by adjusting the height of a water-filled reservoir connected to the back of the pipette. Membrane tension σ was computed from the formula (Waugh and Evans, 1979):

$$\sigma = \Delta P \frac{R_p}{2(1 - R_p/R_v)}, \quad (1)$$

where ΔP is the applied suction pressure, R_p is the inner radius of the pipette, and R_v is the radius of the portion of the vesicle outside of the pipette. Typical values for σ were in the range from 5×10^{-6} to 5×10^{-4} N/m.

Optical tweezers and force calibration

Light from a solid-state, diode-pumped Nd:YAG laser (1064 nm, 2.5 W, continuous wave, Coherent, Saclay, France) was steered into the microscope to generate a single-beam optical trap. The x-y-z position of the trapping zone in the microscope was controlled by means of external optics. Video images of trapped beads (streptavidin polystyrene particles, radius $R = 1.76$ μm) were recorded and analyzed offline using custom-made tracking software (provided by K. Zeldovitch) with a temporal resolution of 40 ms and a subpixel spatial resolution of 35 nm. Trapping stiffness, k_f, was calibrated by measuring the fluctuations of a captured bead for incident laser power lower than 200 mW ($k_f = k_B T/\langle \Delta x^2 \rangle$) and against Stokes' drag force for laser power higher than 200 mW ($k_f \times \Delta x = 6\pi\eta R v$, where Δx is the displacement of the bead in the trap, η is the water viscosity, and v is the velocity of the moving specimen chamber) (Dai and Sheetz, 1995; Bockelmann et al., 2002). From these two methods, the stiffness of the tweezers was found of the order of 0.07 ± 0.01 pN/nm/W. Typical laser powers used in this work were in the 0.5–1 W range.

Coalescence experiments

The crux of our method consisted of pulling simultaneously two tethers from one giant vesicle and getting them to coalesce by moving away the vesicle and thus reducing the distance between the tube-vesicle junctions. Fig. 1 shows a sketch of the whole instrumental setup (Fig. 1 *a*) and a schematic illustration of the coalescence procedure as seen in the microscope (Fig. 1 *b*). As depicted, the vesicle was aspirated and held in a micropipette, one streptavidin bead was captured by optical trapping and a second streptavidin bead was firmly aspirated in a second micropipette, which was maneuvered with a mechanical three-axis micromanipulator (Leica, Wetzlar, Germany). The first tether was formed by bringing the micromanipulated streptavidin bead into contact with the biotinylated vesicle and by retracting the pipette at controlled speed (typically 0.5 μm/s). The second tether between the vesicle body and the optically trapped bead as extruded in the same way. The two beads were finally carefully aligned in the same focus plane and separated by ~10 μm.

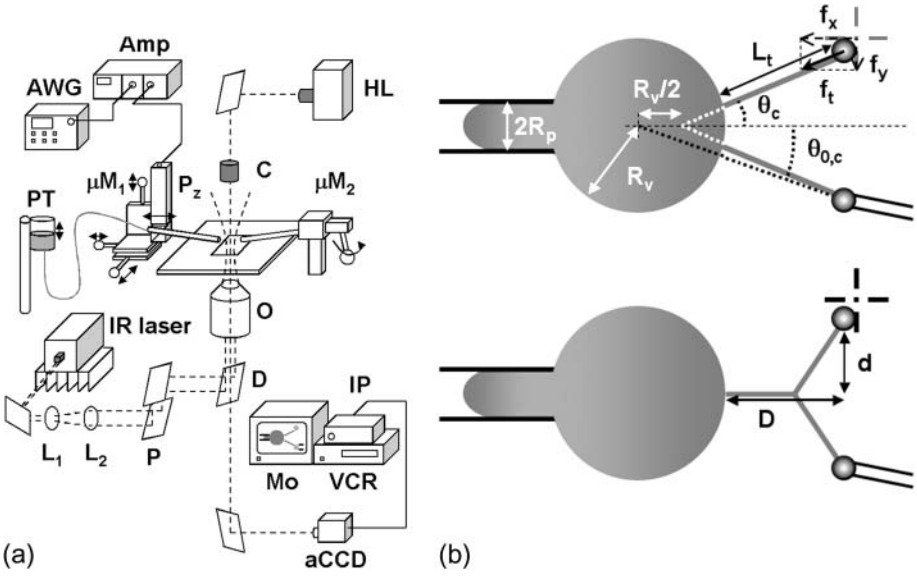

FIGURE 1 (*a*) Complete instrumental apparatus assembled around a bright-field inverted microscope. Light from halogen lamp (*HL*) travels through condenser (*C*) and illuminates the sample. Objective (*O*) collects the images, which are captured by analogic camera (*aCCD*) (25 fps), visualized on control monitor (*Mo*), and recorded with VCR after image processing (*IP*). The arbitrary waveform generator (*AWG*) provides the input signal to high-voltage amplifier (*Amp*), which drives piezo-element (*Pz*). Piezo-translator (*Pz*) is mounted on three-axis micromanipulator ($\mu M1$) and sets the vesicle-holding pipette displacement. Aspiration pressure is controlled by adjusting the elevation of a water tank (*PT*). One bead is held in a pipette that is connected to mechanical micromanipulator μM2. Both μM2 and μM1 are mounted on the stage of the microscope. The second bead is trapped by optical tweezer, which is created by steering light from infrared laser (*IR laser*) into the microscope via external optics including lenses (*L1* and *L2*), periscope (*P*), and dichroic mirror (*D*). (*b*) Schematic of experimental design. (*Top*) A vesicle (radius R_v) is aspirated in a pipette (diameter $2R_p$). Two tethers were extracted from the vesicle, respectively, with the micromanipulated and the optically trapped bead. Length of the nanotubes is L_t. Tether force, f_t, is monitored by optical tracking of the x and y components of bead displacement. In this ''V'' configuration, the half-angle between both tethers is θ. In the Theory section, we used the notation θ_0 for the half-angle between the two radial directions (from the centers of the beads to the center of the vesicle). The vesicle is retracted, which induces a diminution of θ_0, down to a value $\theta_{0,c}$ when coalescence occurs. (*Bottom*) when both tethers merge, a ''Y'' configuration is reached. D and d are the distances that are experimentally measured and will serve for analysis.

The coalescence assay itself consisted in elongating the tethers by retracting slowly along the x axis (either manually or at a constant speed of 0.1 μm/s) the vesicle-holding pipette until both tethers merged from the vesicle body and the resulting three-tube junction moves toward its equilibrium position, close to the beads, to satisfy a zero force condition. Two parameters were measured, namely the force required to form and elongate the tube using the optically trapped bead, and the angle between the two tubes when coalescence occurs. Additionally, in some favorable cases (detailed in the Results section), we also investigated the dynamics of the coalescence process, i.e., the time required for the junction to reach equilibrium. Tracking the x-y position of the optically trapped bead allowed us to monitor the time evolution of the force, $f_t = (f_x^2 + f_y^2)^{1/2}$, applied to the bead during the experiment. The angle, θ, between both tubes was measured by offline image analysis using the public domain software ImageJ. All the data reported in the Results section were obtained for various types of lipid vesicles, in liquid-ordered and liquid-disordered phases, and for various membrane tensions, tuned by micropipette aspiration.

Eventually, we aimed to show how our coalescence procedure could be used to measure the adhesion energy of vesicles to substrates. To do so, we did not use the vesicle-holding pipette and let the biotinylated vesicles sediment and adhere onto streptavidin-coated surfaces. These substrates were prepared by adsorption of polyethylene-imine (PEI) on clean glass coverslides before incubation in a solution of streptavidin (0.1 mg/ml) in PBS. Additionally, the observation chamber was rigidly connected to the long scanning range piezo-actuator to finely control the displacement of the whole chamber in the x direction.

VALIDATION OF THE EXPERIMENTAL SETUP AND FIRST OBSERVATIONS OF TUBE COALESCENCE

As mentioned in the Introduction, there are two widely used micromanipulation methods that provide measurements of the bending rigidity of giant lipid vesicles: the micro-aspiration technique (Evans and Rawicz, 1990; Rawicz et al., 2000) and the tether-pulling method (Heinrich and Waugh, 1996). Because our experimental setup is aimed to: i), study the coalescence of two tethers extracted from a giant vesicle aspirated in a micropipette, and ii), demonstrate how this process can be advantageously used to probe the elastic properties of lipid bilayers, we shall first recall the basics of these two classical micromanipulation methods and validate our setup on vesicles that exhibit well-characterized elastic properties. At the end of this section, our observations on tube coalescence will be presented.

Measurements of bending moduli by micropipette aspiration

Mechanics of pressurized vesicles in micropipettes has been developed and described in detail by Evans et al. (Evans and Skalak, 1980; Needham and Zhelev, 1996). Briefly, direct measurements of aspiration length versus aspiration pressure were converted to apparent area expansion versus tension of bilayers. In the low tension regime, the apparent expansion is dominated by smoothing of thermal undulations and the bending modulus κ is given by the relation (Evans and Rawicz, 1990):

$$\sigma/\sigma_0 \approx \exp[(8\pi\kappa/k_BT)\Delta A/A_0], \quad (2)$$

with σ and σ_0 the actual and initial membrane tensions, k_BT the thermal energy $\sim 4 \times 10^{-21}$ J $= 4$ pN nm, and $\Delta A/A_0$ the fractional increase in apparent area of the vesicle. ΔA was measured from the variation of the displacement ΔL_p of the projection length in the micropipette (Rawicz et al., 2000): $\Delta A \approx 2\pi R_p(1 - R_p/R_v)\Delta L_p$, and A_0, which is the optically measured membrane area at the initial tension σ_0, was calculated from the measured vesicle radius: $A_0 = 4\pi R_v^2$.

In the high-tension regime, the increase $\Delta A'/A_0'$ is due to the elastic stretch of the membrane accompanied with a reduction in lipid surface density. The area-expansion modulus K_a is then given by a linear relation between tension and increase in apparent area: $\sigma = K_a(\Delta A'/A_0')$ (Evans and Skalak, 1980). In the rest of this article, we will only focus on the bending rigidity modulus of bilayer vesicles.

As a standard lipid to calibrate the aspiration system of our setup, we selected EPC. Vesicles thus contained mostly EPC and a small amount of mPEG-DOPE (4.995% molar) and of DSPE-PEG-biotin (0.005% molar) for sake of comparison with further coalescence experiments. Fig. 2 displays a linear plot of tension as a function of apparent area expansion. The solid curve is a fit to the experimental data restricted to the low-tension regime (i.e., $\Delta A/A_0 < 0.025$) using Eq. 2, which yields $\kappa = 11.8 \pm 2.8$ k_BT. By comparison with previously reported values in the literature of the order of 10 k_BT for EPC vesicles (Pécréaux et al., 2004 and references therein), the slight increase observed here can be rationalized by the addition of PEG-lipid. As shown in

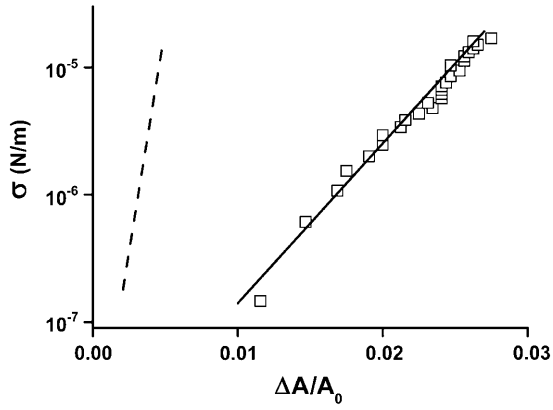

FIGURE 2 Bending rigidity measurements by micropipette aspiration. Semilog plot of tension versus apparent area expansion. Squares are data points obtained for vesicles made from EPC/mPEG-DOPE/DSPE-PEG-biotin (95:4.995:0.005) over tensions from 10^{-7} to 10^{-5} N/m using the micropipette aspiration technique. The exponential rise of tension with area expansion reveals the regime dominated by thermal fluctuations. The solid line is a fit using Eq. 2. The slope yields the bending rigidity $\kappa = 11.8$ k_BT. The dashed line corresponds to the hypothetical variation of tension as a function of area expansion for more rigid vesicles (typically in a liquid-ordered state) ($\kappa = 70$ k_BT). Because the low-tension regime is only accessible for area expansion lower than 0.01, direct measurement of κ for liquid-ordered vesicles is not possible by this method.

Evans and Rawicz (1997), doping lipid bilayers with 5% PEG^{2000}-lipid gives rise to a 1-k_BT increase in elastic bending rigidity, which is fully consistent with our measure of κ.

The microaspiration technique is therefore very convenient to measure bending moduli of fluid bilayers. However, limitations appear when dealing with vesicles characterized by larger bending rigidity. To probe the sole undulation-dominated regime, minuscule apparent area expansions have to be measured precisely. The first limitation is set by the sensitivity of the aspiration device, which is typically restricted to 0.1–0.2 Pa. The second limitation is related to the validity of the relation between σ and ΔP in the low-suction pressure regime. This relation derived from the Laplace equation is strictly valid when the vesicle-cylindrical segment inside the pipette is few times longer than the radius of the pipette. Otherwise, the curvature radius of the aspirated portion of the vesicle may be underestimated. In consequence, microaspiration is generally not well adapted to the determination of bending moduli of ''rigid'' (e.g., liquid-ordered) vesicles. In Fig. 2, the dashed line shows the expected σ–$\Delta A/A_0$ plot for vesicles of $\kappa = 70\ k_BT$ (which is in the range of reported values for liquid-ordered bilayers). The bending-dominated regime is clearly difficult to achieve accurately, given the abovementioned limitations.

Measurements of bending moduli by tether-pulling force experiments

As shown by Heinrich and Waugh (1996), the axial force on a tether extracted from a vesicle, f_t, is proportional to the square root of both the bending stiffness, κ, and the membrane tension, σ, following:

$$f_t = 2\pi\sqrt{2\kappa\sigma}. \quad (3)$$

Here, we adopted a similar approach, but used an optical trap instead of a magnetic tweezer. Our trap was calibrated as described in the Materials and Methods section. The lower curve in Fig. 3 *a* displays a typical force-time trace obtained for a tether extruded from a vesicle composed of EPC/mPEG-DOPE/DSPE-PEG-biotin (95:4.995:0.005) at $v = 0.2$ μm/s. As independently predicted by Powers et al. (2002) and Derényi et al. (2002), the force first grew approximately linearly with the deformation (or time) before reaching a plateau, which yields the equilibrium tether force, f_t. Between these two regimes, a force overshoot was observed, corresponding to the nucleation of the cylindrical tube and relaxation of the vesicle to a more spherical shape. The magnitude of the overshoot was found to be quite variable from one experiment to another, depending on the contact time between the biotinylated vesicle and the streptavidin bead, and thus the size of the adhesion patch, as quantitatively described by the Dogterom group (Koster et al., 2005). We thus investigated ~10 vesicles at different

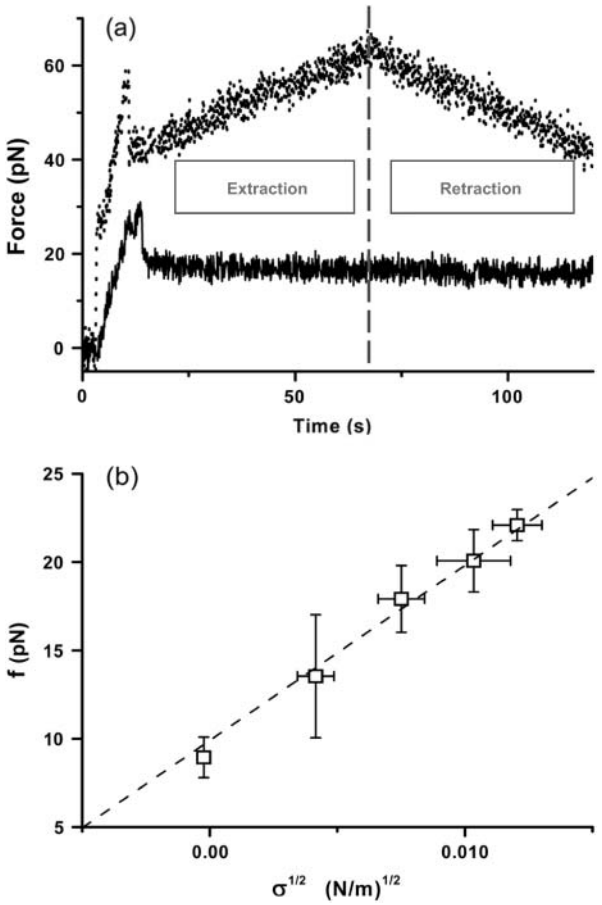

FIGURE 3 Extraction of a single-membrane tether using an optical trap. (*a*) Plots of measured force versus time for fluid (''liquid-disordered'') vesicles made of EPC/mPEG-DOPE/DSPE-PEG-biotin (95:4.995:0.005) (*solid curve*) and for liquid-ordered vesicles made of BSM/cholesterol/mPEG-DOPE/DSPE-PEG-biotin (47.5:47.5:4.995:0.005) (*dotted line*). Tube extraction and retraction are recorded consecutively (end of extraction cycle marked by the *vertical dashed line*). See text for details. (*b*) Plot of the tether force f as a function of the square root of membrane tension σ averaged over 10 vesicles made of EPC/mPEG-DOPE/DSPE-PEG-biotin (95:4.995:0.005). The variation is linear, as predicted by Eq. 3. The slope of the linear fit (*dashed line*) yields the bending rigidity: $\kappa = 12 \pm 1\ k_BT$.

membrane tensions. Fig. 3 *b* displays the force as a function of the square root of the tension. The error bars mainly reflect the average on different vesicles and the variation in membrane tensions from one experiment to another. As expected from Eq. 3, a linear dependence was obtained, and the slope provided the bending modulus $\kappa = 12 \pm 1\ k_BT$, which is in excellent agreement with the value derived from micropipette aspiration.

This tether-pulling approach to measure the bending stiffness of vesicles could in principle be applied to any kind of lipid bilayer. Extraction of a membrane tube from ''rigid'' and highly tense vesicles is possible as long as the power of the trapping laser is high enough to overcome the force overshoot. However, for high values of κ, we might find it difficult to measure the tether force over a large range

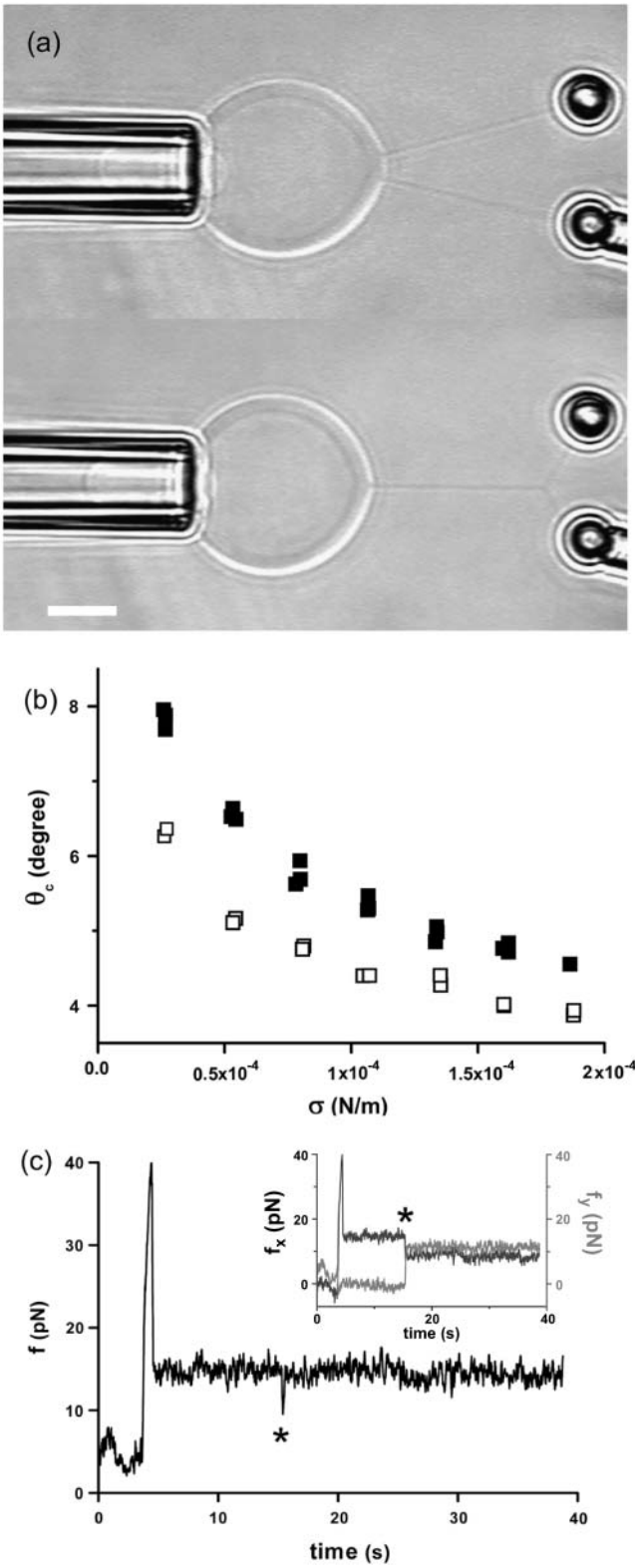

FIGURE 4 Tether coalescence. (*a*) Videomicrographs of the experimental arrangement. The vesicle is aspirated in the left pipette. Two beads serve as handles to extrude tethers from the vesicle. A bead held in a pipette is maneuvered with a micromanipulator. The second bead is trapped in a fixed optical tweezer. The upper image shows the ''V'' configuration, before tube coalescence. The vesicle-holding pipette is retracted until coalescence is triggered. The lower image shows the equilibrium ''Y'' configuration reached after coalescence. Scale bar is 5 μm. (*b*) Plot of the coalescence angle, θ_c, versus membrane tension for two fluid vesicles (EPC/mPEG-DOPE/DSPE-PEG-biotin (95:4.995:0.005)) of different radii (*open squares*, $R_0 = 13$ μm; *solid squares*, $R_0 = 7.5$ μm). (*c*) Typical temporal evolution of the tether force during tubes extraction and coalescence (marked by *asterisk* symbol). The vesicle was made from EPC/mPEG-DOPE/DSPE-PEG-biotin (95:4.995:0.005) and aspirated at $\sigma = 5 \times 10^{-5}$ N/m. The inset shows the *x* and *y* components of the tether force, as derived from the *x*-*y* optical tracking of the bead position. The drop in f_x and the increase in f_y reflect the sudden change in tether orientation after coalescence. The overall tether force after coalescence, $f_t = \sqrt{f_x^2 + f_y^2}$, is the same as before coalescence because the membrane tension is set constant by micropipette aspiration.

of tensions because of the intrinsic limitation of the tension control reported above arising from the breakdown of Eq. 1 when the aspiration length is too small (typically $<2R_p$). The upper curve in Fig. 3 *a* shows a typical force-time curve for a tether extracted at $v = 0.2$ μm/s from a vesicle in a liquid-ordered phase (BSM/cholesterol/mPEG-DOPE/DSPE-PEG-biotin (47.5:47.5:4.995:0.005)) at low membrane tension ($\sigma = 5 \times 10^{-5}$ N/m). As observed, after passing the overshoot, the measured force readily started to increase. This increase was assigned to the fact that the excess area accumulated in the tether was taken from the lipid reservoir of the tongue, leading to a decrease of the aspiration length below the critical threshold of validity of Eq. 1. As a consequence, the radius of curvature of the cylinder cap became larger than the radius of the pipette, and concomitantly, according to Eq. 1, we observed an actual increase of membrane tension (i.e., an increase in the tether force).

The angle between two tethers at which coalescence occurs depends upon the membrane tension

In the previous two paragraphs, we have checked that our microaspiration device was operating properly and that our laser tweezer force measurements were reliable. In the rest of the article, we will focus on the coalescence process of two tethers. As described in the Materials and Methods section, the vesicle was maintained in a micropipette at controlled aspiration pressure, one tether was formed using another micropipette and the force required to form the second tether was measured by monitoring the bead displacement in the optical trap. The snapshots in Fig. 4 *a* are typical videomicrographs taken before and after the coalescence occurred upon retraction of the vesicle-holding pipette. The upper photograph shows the two tethers connected between the vesicle body and each bead. Then, the vesicle was moved back by ~0.2 μm. The lower micrograph shows the resulting ''Y'' tube configuration after coalescence: only one tube is connected to the vesicle, and this tube is further split into two tethers in the vicinity of the beads. As a preliminary

experiment, we measured the angle of coalescence between the two tethers for EPC/mPEG-DOPE/DSPE-PEG-biotin (95:4.995:0.005) vesicles for various membrane tensions. Fig. 4 *b* represents the generic evolution of the coalescence angle, θ_c, as a function of σ for two vesicles of different radii (7.5 and 13 μm). Immediately apparent in Fig. 4 *b*, θ_c decreased with increase in the membrane tension, meaning that coalescence occurred at shorter pipette displacements when the vesicles were tenser. Although small in magnitude, these changes in θ_c are reproducible and easy to detect by image analysis. Simultaneously, the force applied to the trapped bead was measured as a function of time during tube elongation. A typical force-time curve is shown in Fig. 4 *c*. The overall shape is similar to the one obtained for a single tube, with a plateau value located at 15 pN, which is consistent with the equilibrium force of a tether pulled from an EPC vesicle at $\sigma = 5 \times 10^{-5}$ N/m. The only difference lies in the presence of a sudden and transient drop in force around 15 s, when both tubes merged (marked by an *asterisk* symbol). Coalescence is, however, more clearly revealed by direct inspection of the *x* and *y* components of f_t, as displayed in the inset in Fig. 4 *c*, since f_x decreased and f_y increased at the coalescence (corresponding to a global displacement of the trapped bead). As we will show in the Theory section below, the knowledge of tether force and coalescence angle provide a direct determination of the bending modulus and the membrane tension of the vesicle.

THEORY: COALESCENCE OF TWO TETHERS

Fig. 5 is a sketch, which shows the notations used hereafter. As shown by Powers et al. (2002) and Derényi et al. (2002), when a tether is extracted the shape of the vesicle body (far from the tether, where the bending energy is negligible) also becomes slightly deformed, and the angle change $\Delta\varphi(r)$ due to this deformation decays logarithmically as the inverse of the distance r from the tether axis:

$$\Delta\varphi(r) \approx \frac{2R_t}{r}, \tag{4}$$

where

$$R_t = \sqrt{\frac{\kappa}{2\sigma}}, \tag{5}$$

is the radius of the tether. For a spherical vesicle, Eq. 4 can easily be obtained from the requirement that the force $2r\pi\sigma\sin[\varphi(r)]$ exerted by the surface tension along the periphery of any circular cross section (with radius r and perpendicular to the tether axis) of the vesicle be balanced by both the tether force $f_t \equiv 2R_t\pi 2\sigma$ and the force $r^2\pi\sigma 2/R_v$ exerted on the circle by the Laplace pressure ($\sigma 2/R_v$) inside the vesicle:

$$2r\pi\sigma\ \sin[\varphi(r)] = 2R_t\pi 2\sigma\ +\ \frac{2r^2\pi\sigma}{R_v}, \tag{6}$$

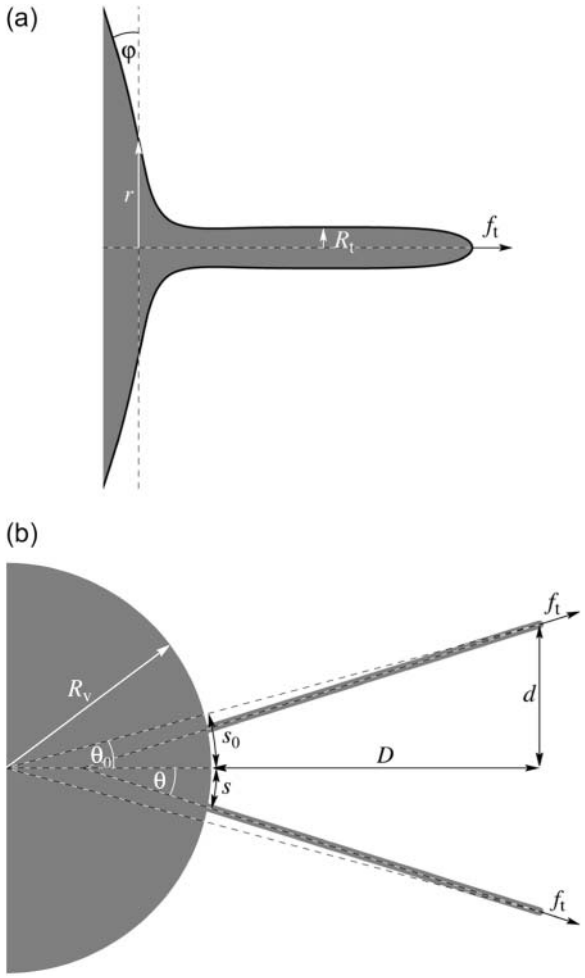

FIGURE 5 (*a*) Qualitative profile of a membrane deformed by the extraction of a tether of radius R_t with a force f_t. The angle φ denotes the absolute angle between the membrane surface and a plane perpendicular to the tether axis, which is located at a distance r. (*b*) Notations defining the relevant geometric parameters. D and d are the experimentally measured distances that allow us to calculate the angle θ and the half-separation s between vesicle-tether junctions. θ_0 and s_0 are the corresponding angle and half-separation in the absence of any surface mediated interaction. R_v is the vesicle radius.

where $\varphi(r)$ denotes the angle between the membrane surface and a plane perpendicular to the tether axis. This equation has also been derived by Bozic et al. (1997), and the shape it describes is called unduloid (or Delaunay surface). For small angles (which is the relevant regime in our experiments) this can be simplified to

$$\varphi(r) \approx \frac{2R_t}{r}\ +\ \frac{r}{R_v}, \tag{7}$$

where the second term corresponds to the undeformed spherical shape of the vesicle and, thus, the first term is indeed the angle change $\Delta\varphi(r)$ induced by the tether extraction.

The necessary condition for a tether to be in equilibrium is that it is perpendicular to the surface of the vesicle (more

precisely, to the original surface, before the tether extraction). Otherwise, the vesicle-tether junction moves in the direction, where the angle between the axis of the tether and the tangent plane of the vesicle is the smallest. Thus, in the absence of any surface-mediated interaction, our two tethers would simply lie in the radial directions connecting the center of the spherical vesicle to the centers of the beads. The half-angle between these two directions would be:

$$\theta_0 = \arctan\left(\frac{d}{R_v + D}\right), \tag{8}$$

and the half-separation between the vesicle-tether junctions:

$$s_0 = R_v\theta_0. \tag{9}$$

But because the membrane at either vesicle-tether junction is slightly deformed by the other tether, the junctions will move toward each other from these interaction-free positions. Because the angle change at the junctions

$$\Delta\varphi_1 \approx \Delta\varphi(2s) \approx \frac{R_t}{s}, \tag{10}$$

monotonically increases as the half-separation s between the junctions decreases, this effect alone would let the tethers coalesce. However, as the junctions approach each other, the tethers get more and more out of the corresponding radial directions, causing their angles to the original spherical surface change by about

$$\Delta\varphi_2 \approx \frac{s_0 - s}{R_v} + \frac{s_0 - s}{L_t} = \frac{s_0 - s}{R_v^{\text{eff}}}, \tag{11}$$

opposite to $\Delta\varphi_1$. The short-hand notation R_v^{eff} is simply defined through $1/R_v^{\text{eff}} = 1/R_v + 1/L_t$. Thus, the junctions stop when the tethers become perpendicular to the surface, i.e., when the two angle changes balance each other: $\Delta\varphi_1 = \Delta\varphi_2$. Taking Eqs. 10 and 11 we get

$$s^2 - s_0 s + R_t R_v^{\text{eff}} = 0. \tag{12}$$

This second-order equation can be solved for s as long as the discriminant $s_0^2 - 4R_tR_v^{\text{eff}}$ is nonnegative. Thus, as the pipette is being retracted and the half-angle $\theta_0 \equiv s_0/R_v$ between the directions of the two beads from the center of the vesicle is decreasing, the two tethers suddenly coalesce when θ_0 reaches

$$\theta_{0,c} \equiv \frac{s_{0,c}}{R_v} = 2\frac{\sqrt{R_tR_v^{\text{eff}}}}{R_v} = 2\sqrt{\frac{R_t}{R_v(1 + R_v/L_t)}}, \tag{13}$$

below which Eq. 11 has no more solution.

This phenomenon allows us to determine the tube radius

$$R_t = \theta_{0,c}^2 R_v \frac{1 + R_v/L_t}{4}, \tag{14}$$

from the measurement of the coalescence angle $\theta_{0,c}$.

Moreover, with the simultaneous measurement of the tether force f_t, we can deduce both the bending rigidity

$$\kappa = \frac{f_tR_t}{2\pi} = f_t\theta_{0,c}^2 R_v(1 + R_v/L_t)\frac{1}{8\pi}, \tag{15}$$

and the surface tension

$$\sigma = \frac{f_t}{4\pi R_t} = \frac{f_t}{\theta_{0,c}^2 R_v(1 + R_v/L_t)}\frac{1}{\pi}, \tag{16}$$

of the membrane.

At the moment of coalescence the solution of Eq. 12 is $s = s_{0,c}/2$, which means that the separation between the junctions is exactly half of what it would be without their attractive interaction. Note that at this moment one can estimate from simple geometry that the half-angle θ_c between the directions of the tethers is related to the half-angle $\theta_{0,c}$ between the directions of the two beads from the center via $\theta_c \approx \theta_{0,c}(1 + R_v/(2L_t))$.

RESULTS AND DISCUSSION

Coalescence tether force and angle yield direct measurements of bending stiffness and membrane tension

We have shown that our experimental setup permits facile measurements of the angle between two tethers and of the force exerted by one tether during the process of tube elongation until coalescence. According to Eqs. 15 and 16, for tubes that are much longer than the size of the vesicle, the product $f_t \times (R_v\theta_{0,c}^2)$ and the ratio $f_t/(R_v\theta_{0,c}^2)$ are expected to be proportional to κ and σ, respectively. For shorter tubes (typically $L_t < 5R_v$), R_v should be replaced by $R_v(1+R_v/L_t) = R_v^2/R_v^{\text{eff}}$, where R_v^{eff} is the effective radius, i.e., the vesicle radius weighted by the length of the tube, according to Eq. 11. Although this correction was systematically computed, the ratio R_v^2/R_v^{eff} will be referred to as «R_v» in the rest of the article for sake of simplicity in the notations.

As a first experiment aimed to demonstrate the validity of this theoretical approach, we used the well-characterized EPC vesicles doped with 5% PEG-lipid (mPEG-DOPE and DSPE-PEG-biotin). We investigated the behavior of eight different vesicles (with radii ranging from 9 to 22 μm) at six different membrane tensions (between 2×10^{-5} and 2×10^{-4} N/m), as controlled by micropipette aspiration. Coalescence events were repeated three times for each vesicle and each tension, at increasing and decreasing aspiration pressures. No observable hysteresis was observed between increasing and decreasing pressures in the force and angle measurements. The results are collected in the graph, Fig. 6. Several remarks can be made here. First, the ratio $f_t/(\pi R_v\theta_{0,c}^2)$, increased linearly with membrane tension with a slope equal to 0.96 ± 0.06, close to unity. Because

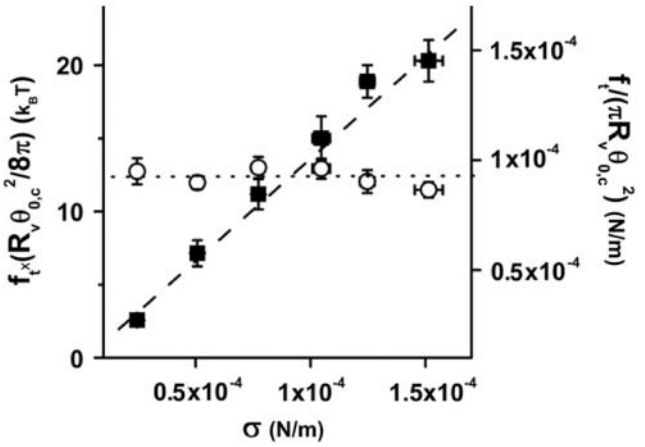

FIGURE 6 Plot of $f_t/(\pi R_v\theta_{0,c}^2)$ (*solid squares*) and $f_t \times (R_v\theta_{0,c}^2/8\pi)$ (*open circles*) versus membrane tension for vesicles made from EPC/mPEG-DOPE/DSPE-PEG-biotin (95:4.995:0.005). Note that R_v was actually corrected by a geometric factor, $(1 + R_v/L_t)$, which is not negligible for tubes that are not much longer than the size of the vesicle (see Theory section for details); f_t is the tether force at coalescence. As expected from Eqs. 15 and 16, $f_t/(\pi R_v\theta_{0,c}^2)$ yields σ, whereas $f_t \times (R_v\theta_{0,c}^2/8\pi)$ represents κ.

$f_t/(\pi R_v\theta_{0,c}^2)$ has the dimensions of a force per unit length, it can be identified with σ, in agreement with Eq. 15. Second, the product $f_t \times (R_v\theta_{0,c}^2/8\pi)$, which is dimensionally equivalent to an energy, was found to remain constant over the explored range of σ. According to Eq. 15, this energy is expected to be the bending rigidity of the vesicles. The average value, $12.3 \pm 0.6\ k_BT$, is indeed consistent with the values of κ that were obtained by either micropipette aspiration or single tube pulling force experiments. These two results correspond very well to the predicted behavior, giving a high level of confidence that the theoretical model properly accounts for the most significant aspects of the process of coalescence.

The uncertainties that must be considered when analyzing the results are mainly threefold. First, the errors in the κ-values may be due to the classical errors of calibration in the trap stiffness of the optical trap. Yet, we checked the calibration of the trap at the beginning and at the end of the series of experiments and we did not notice any change, meaning that an initial error in the calibration could only lead to a systematic shift of the measured forces. Second, because of the smallness of the observed coalescence angles ($\theta \sim 5$–$10°$), minute errors in θ may cause significant uncertainties on κ. Because θ was derived from the mutual distance between beads and the tube length (see Figs. 1 *b* and 4), a way to improve the accuracy of θ measurements would be in principle to increase the separation between beads, and concomitantly the tube lengths. However, for obvious practical reasons, we needed to keep the image of the vesicle-tether junction within the CCD array. This technical condition imposed an optimum distance between beads, of the order of 10 μm in our case. Third, the largest source of error in the measurements presented above was very likely to come from a misalignment of the two beads in the same horizontal plane. A 1-μm difference in elevation was sufficient to underestimate the distance d by ~10%, and subsequently the angle θ. Reproducible measurements of κ were only obtained when careful matching of the two bead images was achieved.

Despite these uncertainties and the apparent more complex geometry, this method offers substantial advantages over previously developed techniques of measuring the bending stiffness of giant vesicles. Because $f_t/(R_v\theta_{0,c}^2)$ directly yields σ, all uncertainties intrinsic to membrane tension estimates by micropipette techniques are immediately eliminated. In particular, errors in pipette radii and aspiration pressure measurements disappear in our approach. More important, the calculation of κ is not tension dependent. In other words, there is no need to control the membrane tension to derive the bending stiffness. This may be of particular interest for rigid bilayers like vesicles in a liquid-ordered phase. Of course, one might argue that the product of the equilibrium tube force by the tube radius is also tension independent ($f_t \times R_t/2\pi = \kappa$). However, values for R_t are typically in the 10–40-nm range, which is not possible to measure reliably by optical methods.

Bending stiffness of liquid-ordered vesicles

Vesicles made of BSM/cholesterol/mPEG-DOPE/DSPE-PEG-biotin (47.5:47.5:4.995:0.005) were shown to be in a L_O phase (Roux et al., 2005; Almeida et al., 2003). We did not manage to measure their bending rigidity by monitoring the membrane tension as a function of the dilatational area using the micropipette technique. Additionally, we found it difficult to measure the equilibrium force of a single tether in the low-tension regime. This tube coalescence method was thus tested on these BSM/cholesterol vesicles. About 40 events were studied for different vesicles and aspiration pressures. Fig. 7 displays the obtained histogram of $\kappa = f_t R_v\theta_{0,c}^2/8\pi$. The peak value was $66 \pm 1 k_BT$, which is significantly larger than the value of 12 k_BT that we found for EPC vesicles. We also checked that $f_t/(\pi R_v\theta_{0,c}^2)$ was increasing linearly (slope 1.06) with the membrane tension σ over the range of aspiration pressures for which the tongue was measurable (data not shown). The method has thus been demonstrated to be successful in determining high bending moduli of lipid bilayers. To our knowledge, not many techniques permit the measurement of large bending rigidities of lipid vesicles. Recently, Lee et al. (2001) have shown that the deformation of a vesicle by a laser beam close to the focal plane could be analyzed with a nanometer resolution with a differential confocal technique and could provide an estimate of the bending modulus with 10% uncertainty. The advantage of this method is that not only the bending rigidity but also the membrane tension can be derived from the coalescence force and angle.

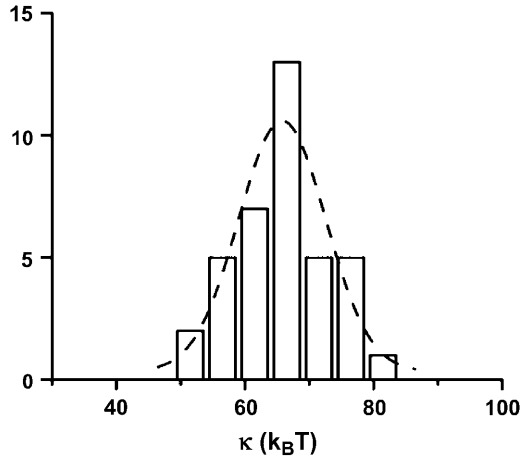

FIGURE 7 Histogram of bending moduli as derived from $\kappa = f_t \times (R_v\theta_{0,c}^2/8\pi)$ for liquid-ordered vesicles (BSM/cholesterol/mPEG-DOPE/DSPE-PEG-biotin (47.5:47.5:4.995:0.005)). The peak value is $\kappa = 66 \pm 1\ k_BT$.

Application to the measurement of vesicle-substrate adhesion energies

A classical method used to measure the adhesion energy of vesicles in contact with surfaces, W, consists of deriving it from the Young-Dupré equation: $W = \sigma(1 - \cos\psi)$. This implies preliminary measurements of the membrane tension σ, and of the contact angle $\psi \approx R_c/R_v$ for small angles, with R_c the radius of the adhesion patch and R_v the vesicle radius. Reflection interference contrast microscopy (RICM) is generally considered the most suitable tool to measure simultaneously ψ and σ. This interferometric technique indeed permits us to visualize adhesion patches as dark spots and to obtain the membrane profile close to the surface from Newton rings patterns. Reconstructing the profiles provides the main two geometric parameters, namely ψ and the capillary length, $\lambda = \sqrt{\kappa/\sigma}$, which is defined by the distance from the rim of the adhesion disk to the intersection of the tangent to the vesicle with the flat substrate (Bruinsma and Sackmann, 2001). One can thus immediately remark that this method: 1), requires the knowledge of κ, and 2), is not applicable for λ values smaller than the optical x-y resolution, practically below ~200 nm. This latter situation corresponds to strong adhesion or relatively tense vesicles ($\sigma > 10^{-6}$ N/m).

The developed tube coalescence method was thus applied to the measure of tensions of adhering vesicles to obtain the adhesion energy density. EPC/mPEG-DOPE/DSPE-PEG-biotin (95:4.995:0.005) vesicles were allowed to sediment on streptavidin-coated substrates (see Materials and Methods). Once the adhesion patch reached its equilibrium size, two tethers were then extruded by displacing the whole stage at constant velocity ($v = 0.2$ μm/s). Fig. 8 *a* displays two videomicrographs taken before tube formation. From the left phase contrast image, R_v was measured. From the right RICM image, the footprint being almost circular, we could measure the adhesion radius, $R_c \approx 3.7$ μm. Fig. 8 *b* shows two phase contrast photographs taken before and after coalescence of the tethers. As explained in the previous paragraphs, the force applied to the bead and the angle between both tubes yield the membrane tension of the vesicle when coalescence occurs. With $\theta_{0,c} = 8°$, $R_v = 9$ μm, and $f_{t,c} = 8.2$ pN, we obtained $\sigma_c = 1.4 \times 10^{-5}$ N/m. To derive the initial tension of the adhered vesicle, we have to take into account the change in σ induced by the relative increase in surface area due to tube extraction. By assuming that fluctuation effects are still dominant (and ignoring the vesicle's stretching component), we may use Eq. 2, which can be written here: $\sigma_c/\sigma_i \approx \exp\ [(8\pi\kappa/k_BT)\Delta A/A_0]$. Neglecting any variation in vesicle size, the relative increase in area is then simply given by: $\Delta A/A = 2 \times 2\pi R_t L/4\pi R_v^2$. Here, the factor 2 accounts for both tethers. The tube radius

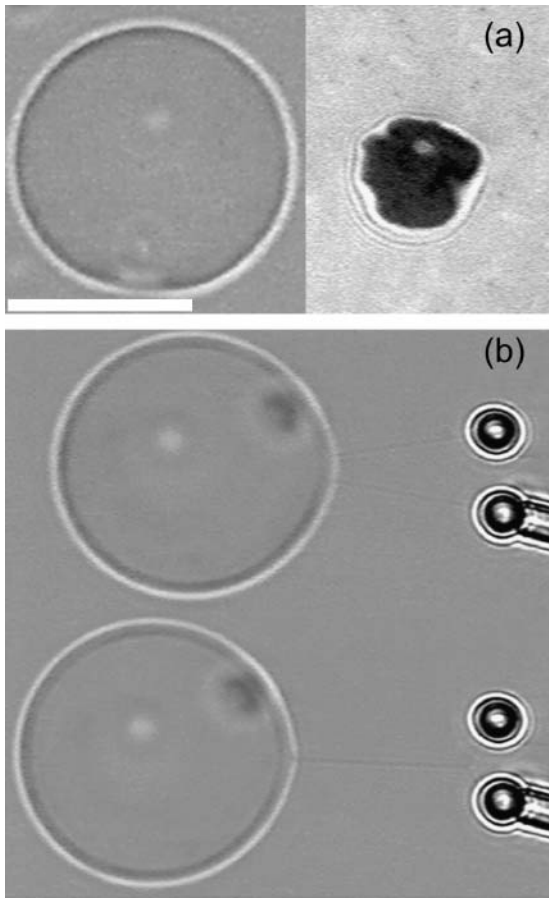

FIGURE 8 Application of the coalescence method to the measurement of adhesion energies of vesicles. (*a*, *left videomicrograph*) Phase contrast image of the equatorial plane of an adhered vesicle (EPC/mPEG-DOPE/DSPE-PEG-biotin (95:4.995:0.005)). (*a*, *right micrograph*) RICM image of the contact zone with the substrate for the same vesicle. Contact radius is measured from the size of the dark spot. (*b*) Extraction and coalescence of two tethers from the adhered vesicle. The microscope stage is moved toward the left. Scale bar is 10 μm.

R_t can be related to the surface tension following: $R_t = (\kappa/2\sigma_c)^{1/2}$. With $L = 19$ μm, we then get: $\sigma_I = 7 \times 10^{-7}$ N/m.

Finally, knowing the initial membrane tension and the substrate-vesicle contact angle ($\psi = 24°$), we get the adhesion energy, $W = 60$ nJ/m^2. Comparison with other values reported in the literature (Cuvelier and Nassoy, 2004; Moy et al., 1999) for biotinylated cell mimics is not straightforward, because W is obviously dependent upon the surface density in biotin groups. De Gennes et al. (2003) argued that, when the stickers are grafted and immobile, W is not given by the difference between the two-dimensional osmotic pressures inside and outside the border of the adhesion disk as proposed by Bell et al. (1984) but is simply the chemical energy ΓU, with Γ the concentration of biotinylated lipids and U the binding energy per streptavidin-biotin bond. Taking $U \approx 25$ kT (Merkel et al., 1999) and $\Gamma \approx 10^{13}$ m^{-2} (for our lipid composition), one should obtain $W = 1$ μJ/m^2. The theoretical upper limit is an order of magnitude larger than our measured value. This discrepancy can be attributed to an incomplete coverage of the surface with streptavidin or a diminished activity of immobilized streptavidin (Cuvelier and Nassoy, 2004).

Dynamics of tether coalescence

To understand further the mechanism of tube coalescence, we attempted to monitor the dynamics of coalescence, i.e., the propagation of the three-way junction toward the equilibrium configuration with the shortest total tube length. The common feature among all the cases that we investigated is that the dynamics was very fast because the final configuration was reached within <1 s.

When vesicles were held in micropipettes, coalescence was completed within one or two video frames, i.e., within <80 ms, over the whole range of accessible membrane tensions, 5×10^{-6} N/m $< \sigma < 5 \times 10^{-4}$ N/m. We were thus not able to record the propagation of the bifurcation point. Intuitively, one might expect that coalescence dynamics will slow down by decreasing σ. Consequently, we used flaccid vesicles and let them weakly adhere to substrates that were sparsely covered with streptavidin. These modified surfaces were prepared by coating glass slides successively with polylysine and a mixture of streptavidin/β-casein (in a typical molar ratio of 1:9). Doing so, surface tensions of adhered vesicles were found to be below 5×10^{-7} N/m (as measured in the previous paragraph). Fig. 9, *a–g*, display a typical sequence composed of tube merging. The initial membrane tension was $\sigma \approx 10^{-7}$ N/m. The time interval between each image was 40 ms. At this low surface tension, coalescence occurred within ~0.25 s. More precisely, the graph in Fig. 9 *h* shows the displacement of the junction between the three tubes, d_t, as a function of time. Whereas equilibrium was indeed reached after <0.3 s, the propagation of the junction was roughly linear with time, and the displacement

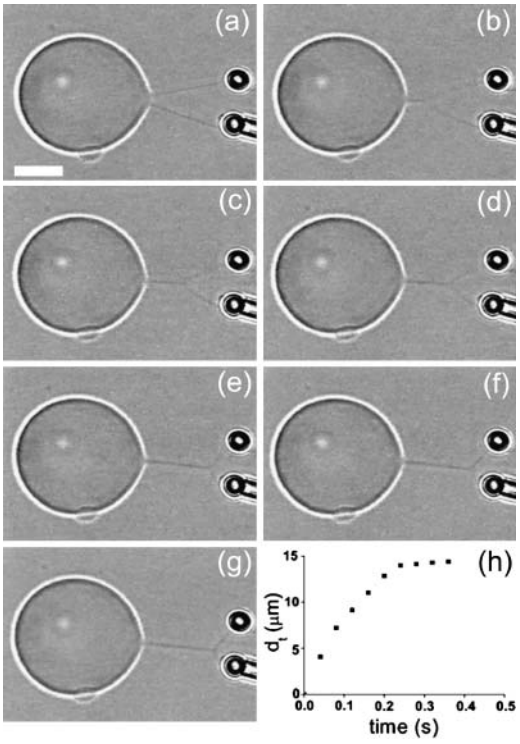

FIGURE 9 Dynamics of coalescence. (*a–g*) Snapshots of tube merging taken at video rate ($\Delta t = 40$ ms). Scale bar is 5 μm. (*h*) Temporal evolution of the position of the three-tube junction during the coalescence process. Initial propagation speed is 80 μm/s.

velocity was of the order of 80 μm/s. Note that Lobovkina et al. (2004) had already described tube coalescence events as elementary steps toward the formation of complex tubular networks. They reported that the equilibrium configuration was reached within ~2 s, which is an order of magnitude slower than the coalescence dynamics measured by us. This difference may come from the protocol of vesicle preparation and tube extrusion. In the experiments performed by the Swedish group (Lobovkina et al., 2004), vesicles of interest are connected to a large reservoir of lipids, which keeps them extremely flaccid, and tethers are formed by a subtle combination of mechanical and electrical, ''patch-clamp like,'' forces. Further experiments and theoretical analysis of the coalescence dynamics are currently under progress.

CONCLUSION

To the best of our knowledge, this work provides the first theoretical and experimental analysis of the coalescence between two membrane tethers. Moreover, we have shown that bending rigidity and membrane tension can be deduced independently from the measure of the angle and tether force at coalescence. In particular, this technique can be equally applied to flexible and rigid membranes. Finally, we have observed that the dynamics of coalescence was extremely

fast. Additional experiments at faster video rate are, however, required for detailed analysis. The results described here could also have implications for biological systems. As commonly believed, tether extraction from living cells induces membrane-cytoskeleton decoupling. However, if tethers were only composed of lipid membrane, they should also merge as observed for phospholipid vesicles, without hysteresis between tube coalescence/tube splitting cycles. Experiments on red blood cells and eukaryotic cells are currently in progress to explore this hypothesis.

We acknowledge the stimulating and helpful conversations with Jean-François Joanny. We are also particularly grateful to Aurélien Roux for his help in the preparation of liquid-ordered vesicles, and to Ulrich Bockelmann for his advice in building our optical trap. I.D. acknowledges support from the Hungarian Science Foundation (Grant No. OTKA F043756) and a Marie Curie European Reintegration Grant (No. 505969). We also receive generous help from the Curie Institute.

This work was supported by the Human Frontier Science Program through research grant No. 52/2003 and ACI Nanosciences-Nanotechnologies (No. NR0032).

REFERENCES

Almeida, R. F. M., A. Fedorov, and M. Prieto. 2003. Sphingomyelin/phosphatidylcholine/cholesterol phase diagram: boundaries and composition of lipid rafts. *Biophys. J.* 85:2406–2416.

Angelova, M. I., and D. S. Dimitrov. 1988. A mechanism of liposome electroformation. *Prog. Colloid Poymr. Sci.* 76:59–67.

Bell, G. I., M. Dembo, and P. Bongrand. 1984. Cell adhesion. Competition between nonspecific repulsion and specific bonding. *Biophys. J.* 45: 1051–1064.

Bockelmann, U., Ph. Thomen, B. Essevez-Roulet, V. Viasnoff, and F. Heslot. 2002. Unzipping DNA with optical tweezers: high sequence sensitivity and force flips. *Biophys. J.* 82:1537–1553.

Brochard, F., and J. F. Lennon. 1975. Frequency spectrum of the flicker phenomenon in erythrocytes. *J. Phys. (Paris).* 36:1035–1047.

Bozic, B., S. Svetina, and B. Zeks. 1997. Theoretical analysis of the formation of membrane microtubes on axially strained vesicles. *Phys. Rev. E.* 55:5834–5842.

Bruinsma, R., and E. Sackmann. 2001. Bioadhesion and the dewetting transition. *C. R. Acad. Sci. Paris. Série IV.* 2:803–815.

Cuvelier, D., and P. Nassoy. 2004. Hidden dynamics of vesicle adhesion induced by specific stickers. *Phys. Rev. Lett.* 93:228101.

Dabora, S. L., and M. P. Sheetz. 1988. The microtubule-dependent formation of a tubulovesicular network with characteristics of the ER from cultured cell extracts. *Cell.* 54:27–35.

Dai, J., and M. P. Sheetz. 1995. Mechanical properties of neuronal growth cone membranes studied by tether formation with laser optical tweezers. *Biophys. J.* 68:988–996.

Dai, J., and M. P. Sheetz. 1999. Membrane tether formation from blebbing cells. *Biophys. J.* 77:3363–3370.

Davidson, M., M. Karlsson, J. Sinclair, K. Sott, and O. Orwar. 2003. Nanotube-vesicle networks with functionalized membranes and interiors. *J. Am. Chem. Soc.* 125:374–378.

De Gennes, P.-G., P.-H. Puech, and F. Brochard-Wyart. 2003. Adhesion induced by mobile stickers: a list of scenarios. *Langmuir.* 19:7112–7119.

Derényi, I., F. Jülicher, and J. Prost. 2002. Formation and interaction of membrane tubes. *Phys. Rev. Lett.* 88:238101.

Dimova, R., B. Pouligny, and C. Dietrich. 2000. Pretransitional effects in dimyristoylphosphatidylcholine vesicle membranes: optical dynamometry study. *Biophys. J.* 79:340–356.

Döbereiner, H.-G., E. Evans, M. Kraus, U. Seifert, and M. Wortis. 1997. Mapping vesicle shapes into the phase diagram: a comparison of experiment and theory. *Phys. Rev. E.* 55:4458–4474.

Evans, E., H. Bowman, A. Leung, D. Needham, and D. Tirrell. 1996. Biomembrane templates for nanoscale conduits and networks. *Science.* 273:933–935.

Evans, E., and D. Needham. 1987. Physical properties of surfactant bilayer membranes: thermal transitions, elasticity, rigidity, cohesion, and colloidal interactions. *J. Phys. Chem.* 91:4219–4228.

Evans, E., and W. Rawicz. 1990. Entropy-driven tension and bending elasticity in condensed-fluid membranes. *Phys. Rev. Lett.* 64:2094–2097.

Evans, E., and W. Rawicz. 1997. Elasticity of ''fuzzy'' biomembranes. *Phys. Rev. Lett.* 79:2379–2382.

Evans, E., and R. Skalak. 1980. Mechanics and Thermodynamics of Biomembranes. CRC Press, Boca Raton, FL.

Evans, E. A., and A. Yeung. 1994. Hidden dynamics in rapid changes of bilayer shape. *Chem. Phys. Lipids.* 73:39–56.

Faucon, J. F., M. D. Mitov, P. Meleard, I. Bivas, and P. Bothorel. 1989. Bending elasticity and thermal fluctuations of lipid membranes: theoretical and experimental requirements. *J. Phys. (Paris).* 50:2389–2414.

Heinrich, V., B. Bozic, S. Svetina, and B. Zeks. 1999. Vesicle deformation by an axial load: from elongated shapes to tethered vesicles. *Biophys. J.* 76:2056–2071.

Heinrich, V., and R. E. Waugh. 1996. A piconewton force transducer and its application to measurement of the bending stiffness of phospholipid membranes. *Ann. Biomed. Eng.* 24:595–605.

Hochmuth, R. M., N. Mohandas, and P. L. Blackshear, Jr. 1973. Measurement of the elastic modulus for red cell membrane using a fluid mechanical technique. *Biophys. J.* 13:747–762.

Hochmuth, R. M., J. Y. Shao, J. Dai, and M. P. Sheetz. 1996. Deformation and flow of membrane into tethers extracted from neuronal growth cones. *Biophys. J.* 70:358–369.

Karlsson, A., M. Karlsson, R. Karlsson, K. Sott, A. Lundquist, M. Tokarz, and O. Orwar. 2003a. Nanofluidic networks based on surfactant membrane technology. *Anal. Chem.* 75:2529–2537.

Karlsson, R., A. Karlsson, and O. Orwar. 2003b. Formation and transport of nanotube-integrated vesicles in a lipid bilayer network. *J. Phys. Chem. B.* 107:11201–11207.

Karlsson, M., K. Sott, M. Davidson, A.-S. Cans, P. Linderholm, D. Chiu, and O. Orwar. 2002. Formation of geometrically complex lipid nanotube-vesicle networks of higher-order topologies. *Proc. Natl. Acad. Sci. USA.* 99:11573–11578.

Koster, G., A. Cacciuto, I. Derényi, D. Frenkel, and M. Dogterom. 2005. Force barriers for membrane tube formation. *Phys. Rev. Lett.* 94:068101.

Koster, G., M. VanDuijn, B. Hofs, and M. Dogterom. 2003. Membrane tube formation from giant vesicles by dynamic association of motor proteins. *Proc. Natl. Acad. Sci. USA.* 100:15583–15588.

Lee, C.-H., W.-C. Lin, and J. Wang. 2001. All-optical measurements of the bending rigidity of lipid-vesicle membranes across structural phase transitions. *Phys. Rev. E.* 64:020901.

Lobovkina, T., P. Dommersnes, J.-F. Joanny, P. Bassereau, M. Karlsson, and O. Orwar. 2004. Mechanical tweezer action by self-tightening knots in surfactant nanotubes. *Proc. Natl. Acad. Sci. USA.* 101:7949–7953.

Merkel, R., P. Nassoy, A. Leung, K. Ritchie, and E. Evans. 1999. Energy landscapes of receptor-ligand bonds explored with dynamic force spectroscopy. *Nature.* 397:50–53.

Moy, V. T., Y. Jiao, T. Hillmann, H. Lehmann, and T. Sano. 1999. Adhesion energy of receptor-mediated interaction measured by elastic deformation. *Biophys. J.* 76:1632–1638.

Needham, D., and D. V. Zhelev. 1996. The mechanochemistry of lipid vesicles examined by micropipet manipulation techniques. *In* Vesicles. M. Rossof, editor. Marcel Dekker, New York, Basel, and Hong Kong. 373–444.

Pécréaux, J., H.-G. Dôbereiner, J. Prost, J.-F. Joanny, and P. Bassereau. 2004. Refined contour analysis of giant unilamellar vesicles. *Eur. Phys. J. E.* 13:277–290.

Powers, T. R., G. Huber, and R. E. Goldstein. 2002. Fluid-membrane tethers: minimal surfaces and elastic boundary layers. *Phys. Rev. E.* 65: 041901.

Rawicz, W., K. C. Olbrich, T. McIntosh, D. Needham, and E. Evans. 2000. Effect of chain length and unsaturation on elasticity of lipid bilayers. *Biophys. J.* 79:328–339.

Roux, A., G. Cappello, J. Cartaud, J. Prost, B. Goud, and P. Bassereau. 2002. A minimal system allowing tubulation with molecular motors pulling on giant liposomes. *Proc. Natl. Acad. Sci. USA.* 99:5394–5399.

Roux, A., D. Cuvelier, P. Nassoy, J. Prost, P. Bassereau, and B. Goud. 2005. Role of curvature and phase transition in lipid sorting and fission of membrane tubes. *EMBO J.* In press.

Rustom, A., R. Saffrich, I. Markovic, P. Walther, and H.-H. Gerdes. 2004. Nanotubular highways for intercellular organelle transport. *Science.* 303:1007–1010.

Sheetz, M. P. 2001. Cell control by membrane cytoskeleton adhesion. *Nat. Rev. Mol. Cell Biol.* 2:392–396.

Svetina, S., B. Zeks, R. E. Waugh, and R. M. Raphael. 1998. Theoretical analysis of the effect of the transbilayer movement of phospholipid molecules on the dynamic behavior of a microtube pulled out of an aspirated vesicle. *Eur. Biophys. J.* 27:197–209.

Terasaki, M., L. B. Chen, and K. Fujiwara. 1986. Microtubules and the endoplasmic reticulum are highly interdependent structures. *J. Cell Biol.* 103:1557–1568.

Upadhyaya, A., and M. P. Sheetz. 2004. Tension in tubulovesicular networks of Golgi and endoplasmic reticulum membranes. *Biophys. J.* 86:2923–2928.

Vale, R. D., and H. Hotani. 1988. Formation of membrane networks in vitro by kinesin-driven microtubule movement. *J. Cell Biol.* 107:2233–2241.

Waugh, R. E., and R. G. Bauserman. 1995. Physical measurements of bilayer-skeletal separation forces. *Ann. Biomed. Eng.* 23:308–321.

Waugh, R., and E. A. Evans. 1979. Thermoelasticity of red blood cell membrane. *Biophys. J.* 26:115–132.

Waugh, R. E., and R. M. Hochmuth. 1987. Mechanical equilibrium of thick hollow liquid membranes cylinders. *Biophys. J.* 52:391–400.